Published in final edited form as:
Environ Sci Technol. 2009 August 1; 43(15): 5671–5678.

CHARACTERIZING PORE-SCALE DISSOLUTION OF ORGANIC IMMISCIBLE LIQUID IN A POORLY-SORTED NATURAL POROUS MEDIUM

A.E. Russo[1], **M. Narter**[1], and **M.L. Brusseau**[1,2,*]

[1]Department of Soil, Water and Environmental Science, University of Arizona, 429 Shantz Bldg., Tucson, AZ 85721

[2]Department of Hydrology and Water Resources, University of Arizona, 429 Shantz Bldg., Tucson, AZ 85721

Abstract

Synchrotron X-ray microtomography was used to characterize the pore-scale morphology and distribution of an organic immiscible liquid (trichloroethene) during water flushing to examine dissolution dynamics. The experiments were conducted with a natural porous medium that has a large particle-size distribution. The results were compared to those of a previous experiment conducted with a well-sorted natural sand. The median organic-liquid blob volume was smaller, and smaller blobs composed a larger fraction of the distribution, for the poorly-sorted medium. In addition, mass removal was less spatially uniform for the poorly-sorted medium. The concentration of trichloroethene in the column effluent was monitored during dissolution to assess mass-flux behavior. A first-order mass transfer equation was used to simulate the measured elution curves. Organic-liquid/water interfacial areas measured with microtomography were used as input, and simulated effluent concentrations were compared to the measured effluent concentrations to determine best-fit values for the mass-transfer coefficient. The value obtained for the poorly-sorted medium was approximately 10 times smaller than that obtained for the well-sorted medium. This disparity indicates that hydraulic accessibility of the organic liquid is more constrained for the poorly-sorted medium, which would be consistent with a more complex pore-scale flow field for the poorly-sorted medium.

INTRODUCTION

Organic immiscible liquids are a persistent source of contamination at many hazardous waste sites. Understanding the distribution and mass-transfer dynamics of these contaminants will allow for better site characterization and determination of applicable remediation technologies. Numerous experiments have been conducted at the column and intermediate scale to investigate the dissolution behavior of organic liquids in porous media (e.g., 1–16). This research has provided significant insight into dissolution dynamics and mass–flux behavior. However, much of this research has been conducted using relatively ideal porous media (e.g., well-sorted sand), while relatively few experiments have been conducted using natural soils and aquifer sediments.

The elution curves for column-scale dissolution experiments conducted with well-sorted sand are typically characterized by an extended steady-state stage, comprising concentrations equivalent to aqueous solubility, followed by a transient stage comprising a

*Corresponding author brusseau@ag.arizona.edu.

rapid decrease in concentration (Figure 1). In contrast, significantly different dissolution behavior has been observed for experiments conducted with poorly-sorted media, as illustrated in Figure 1 (17). This nonideality manifests as multi-step elution curves, wherein there are two or more periods of relatively constant contaminant flux as opposed to the single steady-state stage observed for the well-sorted media. It is hypothesized that the configuration of the flow field and of the immiscible liquid, and concomitantly, dissolution dynamics, is more complex for more poorly sorted media. Mathematical models that account for non-uniform distributions or configurations of organic liquid at the local (column) scale have been developed and used to examine their impact on organic-liquid dissolution (e.g.,3,8,18–21). However, a comprehensive examination of the fundamental processes influencing dissolution requires direct characterization of the pore-scale configuration and distribution of fluids and of fluid-fluid interfaces, and their changes in response to mass-removal events.

The pore-scale morphology and configuration of immiscible liquids have been characterized with several methods, including polymerization techniques, micromodels, and high-resolution imaging. A few recent studies have used advanced imaging to examine organic-liquid dissolution at the pore scale (22–26). The results of these studies have demonstrated the utility of advanced imaging for characterizing pore-scale dissolution dynamics. However, these studies were conducted with glass beads or silica sands. In addition, effluent concentrations (mass flux) were not measured for most of these studies. In this study, dissolution experiments were conducted using a poorly-sorted medium to examine dissolution behavior for a more complex natural porous medium. Synchrotron X-ray microtomography was used to characterize pore-scale organic-liquid morphology and distribution as a function of dissolution. Effluent concentration data were collected to integrate dissolution dynamics with mass-flux behavior.

MATERIALS AND METHODS

Materials

Trichloroethene (TCE) (Aldrich Chemical Co., Inc, Milwaukee, WI) was used as the model organic liquid. To enhance image contrast, trichloroethene was doped with iodobenzene (8% by volume) in the same manner as done by Schnaar and Brusseau (26). The results of prior work has shown that addition of the dopant has minimal impact on fluid configuration and distribution (26,27). Hayhook soil collected from Pima County, AZ was used as the porous medium. It is composed of 85.5% sand, 4.3% silt, 10.2% clay, and 0.08% organic matter. It has a porosity of 0.38, a median grain diameter of 0.26 mm and a uniformity coefficient of 16. The results of a previous experiment conducted with a well-sorted sand was used for comparison (26). The sand has a porosity of 0.33, a median grain diameter of 0.35 mm, and a uniformity coefficient of 1. Aluminum columns, 4.4 cm long and 0.6 cm inner diameter, were used for the experiments to accommodate the imaging.

Experiment Methods

Two dissolution experiments were conducted using the Hayhook soil for which synchrotron X-ray microtomography was employed to image the system. Minimal effluent samples were collected for the initial experiment, and thus this experiment is not used in the quantitative analyses presented below. The results obtained for the second Hayhook experiment are compared to results reported previously for experiments conducted with a well-sorted sand (26).

To ensure a homogeneous pack, the columns were packed in steps by adding a small amount of porous media at a time. After packing, CO_2 was injected into the columns to displace

entrapped air, after which the columns were saturated with de-aired water. Complete saturation was assumed once a constant mass was attained for the column. Saturation conditions were examined afterward using the image data. To establish residual saturation of the organic liquid, approximately one pore volume of liquid-phase TCE was injected into the bottom of the vertically placed column using a gas tight syringe attached to a syringe pump (Sage Model 355). Following the injection, the mobile-phase TCE was removed via insertion of two pore volumes of a saturated TCE solution into the top of the column at a low flow rate, followed by a few pore volumes at a flowrate slightly larger than that used for the dissolution experiment. The capillary number for this displacement process was approximately 10^{-6}, which is consistent with previously published studies. The saturation was determined from analysis of the image data.

Dissolution was initiated by flushing the column with de-aired water at a flowrate equivalent to a mean pore-water velocity of approximately 30 cm/hr, such that dissolution-induced mass removal was examined under induced-gradient conditions such as those associated with pump-and-treat applications. Water was pumped into the column from the bottom (the same direction in which immiscible liquid was injected into the column) using an HPLC pump. Effluent samples were collected with glass syringes (Popper & Sons, Inc, New Hyde Park, N.Y.) and placed in glass sample vials for analysis.

Aqueous TCE samples were analyzed using gas chromatography (GC). Samples, ranging in concentrations from saturation (1300–1400 mg/L) to approximately 10 mg/L were analyzed using a GC-FID (flame ionization detector). A GC-ECD (electron capture detector) with headspace autosampler was used to analyze samples for TCE below 10 mg/L. The oven temperature was held at 40 °C for 2 minutes and then increased at a rate of 10 °C/min to a final temperature of 170 °C. The injector temperature was set at 180 °C, and the detector temperature was set at 200 °C. The quantifiable detection limits were approximately 0.5 mg/L and 0.5 μg/L, respectively.

Simulated column effluent concentrations were calculated using the following equation, assuming one-dimensional transport and steady-state, first-order mass transfer:

$$\frac{C_{x=L}}{C_{sol}} = 1 - \exp\left(-\frac{kA_{nw}L}{q}\right) \quad [1]$$

where q is the Darcy flux (L/T), $C_{x=L}$ is the aqueous-phase concentration of the organic liquid (M/L^3), k is the mass-transfer coefficient (L/T), C_{sol} is the solubility of the organic liquid in the aqueous phase (initial equilibrium concentration) (M/L^3), A_{nw} is the specific organic-liquid/water interfacial area (1/L) and L is the length of the porous-medium zone (L). The solution is derived based in part on an assumption that spreading is insignificant, which is true for these systems. All variables in the r.h.s of Equation 1 are known a priori except for k (where A_{nw} is obtained from microtomography). Simulated effluent concentrations were compared to the measured effluent concentrations to determine best-fit values for the mass-transfer coefficient.

Synchrotron Microtomography

Synchrotron X-ray microtomography was conducted at the GeoSoilEnviroCARS (GSECARS) bending magnet beam-line 13-BM-D (sector 13 at the Advanced Photon Source). Columns were scanned in intervals, each 0.5-cm long. A total of 720 scans were collected for each interval (0.5-degree rotations). Images of the columns were collected sequentially below and above the iodine K-edge (33.0169 and 33.269 keV) to specifically resolve the organic liquid. The entire section of the columns containing porous media was

imaged to determine organic-liquid configuration throughout the column. An initial scan was taken before initiating the experiment, followed by a second scan approximately six hours after the start of the experiment. The experiment was stopped, the column securely capped and then taken to the hutch for imaging. Following the imaging, dissolution was resumed, and a third scan was taken approximately six hours later. Each imaging series took approximately three hours to complete.

The two-dimensional data sets obtained from the imaging were preprocessed and reconstructed to construct three-dimensional image arrays (28). Spatial resolution of the images was approximately 11 μm, allowing for an effective resolution with respect to blob volume of approximately 10^{-5} mm^3. The software package Blob3D, developed specifically for high resolution X-ray microtomography data (29), was used for additional image processing and extraction of quantitative information, including fluid volumes, surface areas, and interfacial areas, as described previously (26,27). The interfacial areas reported herein are total areas, incorporating the contributions of both capillary-associated and film-associated areas. It is important to note that the interfacial areas measured with the microtomography method do not incorporate area associated with microscopic surface roughness (30–32).

RESULTS AND DISCUSSION

Synchrotron X-ray imaging produced data from which the three phases are readily discerned (see Figure 2). Analysis of the microtomography data collected from the initial scan (prior to dissolution) showed that there was no air present in the column. The organic liquid was distributed throughout the width and length of the column, with no preferential occurrence near the walls or in the center. The organic-liquid blobs varied in shape from small spheroidal singlets to larger, more complex ganglia, as observed in prior studies (e.g., 22–27, 33). The distribution of blob shapes and sizes is illustrated in Figure 3, where the surface-area-to-volume ratio is presented as a function of blob volume. The surface-area-to-volume ratio function for a perfect sphere is plotted for comparison purposes. A larger fraction of blobs have surface-area-to-volume ratios closer to that of a sphere at smaller blob volumes ($<10^{-4}$ mm^3). As blob volume increases, the fraction of blobs with surface-area-to-volume ratios greater than that of a sphere increases, indicating more complex blob shapes.

The second scan for the Hayhook column was conducted after approximately 95 pore volumes of water flushing. As expected, the total organic-liquid volume in the system decreased from the initial to the second scan (Table 1). However, the TCE concentrations in the effluent remained at steady-state during this period, with no significant difference in concentration between the initial and second scan. Conversely, a noticeable difference was observed between the second and third scan, which occurred after approximately 185 pore volumes of flushing, wherein the effluent concentration decreased by approximately 50%. As illustrated in Figure 3, the number of blobs decreased in each successive scan, as expected.

Comparison of aggregate data shows that the global surface-area-to-volume ratio for the organic-liquid blobs is significantly greater for the Hayhook soil versus the sand (Table 1). This is a reflection primarily of the much smaller median blob diameter for the Hayhook medium. The cumulative blob-size distributions for both media are shown in Figure 4 for all three scans. Comparison of the two distributions shows that smaller blobs composed a larger fraction of the distribution for the Hayhook medium. The overall distribution of blobs, as well as the SA/Vol ratios (Table 1), did not change significantly during the dissolution process for either medium. The median blob size for Hayhook remained essentially the same between the first and third scans, while it decreased for the well-sorted sand (Table 1, Figure

4). Note that similar mass removals are attained for scan 3 of Hayhook and scan 2 of the well-sorted sand.

Microtomography results for each imaged interval of the column (1–7) for each scan set are reported in Table 2 for the two experiments. This includes values for organic-liquid saturation (S_n) and specific organic-liquid/water interfacial area (A_{nw}). Changes in organic-liquid distribution during the experiments (i.e. in-situ spatially-distributed mass-removal behavior) can be evaluated by examining the data for the individual intervals. For ideal dissolution, the dissolution front is expected to propagate uniformly down-gradient (away from the influent end), with organic-liquid blobs nearest to the influent end of the column being completely removed prior to the dissolution of down-gradient blobs.

For the well-sorted sand, the organic-liquid saturation decreased significantly for each interval between scans 1 and 2 and between scans 2 and 3. The mass removal was greater for the intervals nearer to the influent end, as would be expected. For the Hayhook column, mass removal was progressively less for the intervals farther away from the influent end, with the exception of the farthest three intervals. For example, no measurable mass was removed for interval 2 between scans 1 and 2. However, there was mass removal for interval 1, which is farther downgradient, during that period. Thus, it appears that the dissolution front propagated less uniformly for the Hayhook system than it did for the well-sorted sand. Similar results were observed for the other dissolution experiment conducted using the Hayhook soil (data not shown). Inspection of the image data indicates that the blobs that were bypassed were distributed throughout the column cross section, and not concentrated along the walls. This indicates that the observed bypassing, which is likely associated with hydraulic-accessibility constraints, is not due solely to wall effects.

The elution curves obtained from the dissolution experiments for both media are presented in Figure 5. As discussed above and illustrated in Figure 1, nonideal dissolution behavior manifested as multi-step elution curves is observed for the Hayhook soil (poorly sorted medium), whereas ideal behavior is observed for the well-sorted sand. Time constraints associated with the imaging process did not allow the dissolution experiments presented herein to be conducted to complete mass removal. Therefore, the elution curve obtained for the Hayhook imaging experiment is truncated (Figure 5), and insufficient to allow observation of possible nonideal behavior such as illustrated in Figure 1. However, multiple experiments performed under conditions similar to those in this study, but conducted to complete mass removal, did show nonideal behavior similar to that illustrated in Figure 1 (17).

The elution curves simulated with equation 1 and a constant mass-transfer coefficient (k) are compared to the measured elution curves in Figure 5. The simulated elution curves extend only to the pore volume associated with the last measured interfacial area obtained from the microtomographic imaging, whereas effluent samples were collected after the final scan, represented by the measured values in the figure. The simulated curves match the measured data relatively well. For typical modeling of organic-liquid dissolution, a lumped dissolution rate coefficient ($k_r = kA_{nw}$) is used because interfacial area data are generally unavailable. For such applications, the lumped rate coefficient is treated as temporally variable to account for the decrease in interfacial area as a function of mass removal. The results obtained herein indicate that k is constant (at least over the range investigated), and that measured interfacial area data as a function of mass removal are sufficient to simulate mass removal and mass flux for each porous medium.

The mass-transfer coefficient obtained for the Hayhook dissolution experiment using equation 1 was 0.22 (±0.04) cm/hr. The *k* value obtained for this poorly-sorted medium is

approximately 10 times smaller than that obtained for the well-sorted sand (1.9 ±0.3 cm/hr). The disparity between the two values may in part be due to the fact that Eq. 1 does not include an explicit description of the pore-scale flow field. Thus, the influence of flow-field nonideality and its associated impacts on hydraulic accessibility of the organic phase for dissolution is incorporated into *k*. For example, the significance of diffusion-controlled dissolution domains, wherein direct contact between primary channels of water flow and organic liquid is constrained, are likely to be greater for systems comprising more complex pore-scale flow fields. This and other hydraulic-accessibility constraints are expected to be greater for more heterogeneous, poorly-sorted media.

Organic-liquid dissolution experiments were conducted with a poorly-sorted natural soil, and the results compared to those obtained previously for a well-sorted sand. Synchrotron X-ray microtomography was used to characterize the pore-scale morphology and distribution of the organic liquid as a function of dissolution. Differences were observed between the well-sorted and poorly-sorted media with respect to temporal propagation of the dissolution front. In addition, there was a significant difference in the magnitudes of the first-order mass-transfer coefficients obtained from analysis of the effluent concentration data. These observations are hypothesized to result from a more complex organic-liquid configuration and associated pore-scale velocity field for the poorly-sorted medium. The results of this study illustrate the value of synchrotron X-ray microtomographic imaging for characterizing pore-scale dissolution dynamics in a natural porous medium.

Acknowledgments

This research was supported by the NIEHS Superfund Basic Research Program (Grant # ESO4940). We thank Hilary Janousek, Justin Marble, and Erica DiFilippo for help with collection of the imaging data and sample analysis. Imaging experiments were performed at GeoSoilEnviroCARS (Sector 13), Advanced Photon Source (APS), Argonne National Laboratory. GeoSoilEnviroCARS is supported by the National Science Foundation - Earth Sciences (EAR-0217473), Department of Energy - Geosciences (DE-FG02-94ER14466) and the State of Illinois. Use of the APS was supported by the U.S. Department of Energy, Office of Science, Office of Basic Energy Sciences, under Contract No. W-31-109-ENG-38. We thank Dr. Mark Rivers for his assistance and support. We thank the reviewers for their constructive comments.

Literature Cited

1. Hunt JR, Sitar N, Udell KS. Nonaqueous phase liquid transport and cleanup 2. experimental studies. Water Resour. Res. 1988; 24(8):1259–1269.
2. Miller CT, Poirier-McNeill MM, Mayer AS. Dissolution of trapped nonaqueous phase liquids: mass transfer characteristics. Water Resour. Res. 1990; 26:2783–2796.
3. Borden RC, Kao CM. Evaluation of groundwater extraction for remediation of petroleum-contaminated aquifers. Water. Environ. Res. 1992; 64:28–36.
4. Powers SE, Abriola LM, Weber WJ Jr. An experimental investigation of nonaqueous phase liquid dissolution in saturated subsurface systems: steady state mass transfer rates. Water Resour. Res. 1992; 28(10):2691–2705.
5. Gellar JT, Hunt JR. Mass transfer from nonaqueous phase organic liquids in water-saturated porous media. Water Resour. Res. 1993; 29(4):833–845. [PubMed: 20336189]
6. Imhoff PT, Jaffe PR, Pinder GF. An experimental study of complete dissolution of a nonaqueous phase liquid in saturated porous media. Water Resour. Res. 1994; 30(2):307–320.
7. Powers SE, Abriola LM, Webber WJ Jr. An experimental investigation of nonaqueous phase liquid dissolution in saturated subsurface systems: transient mass transfer rates. Water Resour. Res. 1994; 30:321–332.
8. Rixey WG. The long-term dissolution characteristics of a residually trapped BTX mixture in soil. Haz. Waste and Haz. Mat. 1996; 13:197–211.
9. Fortin J, Jury WA, Anderson MA. Dissolution of trapped nonaqueous phase liquids in sand columns. J. Env. Quality. 1998; 27:38–45.

10. Imhoff PT, Arthur MH, Miller CT. Complete dissolution of trichloroethylene in saturated porous media. Environ. Sci. Technol. 1998; 32:2417–2424.
11. Powers SE, Nambi IM, Curry GW Jr. Non-aqueous phase liquid dissolution in heterogeneous systems: mechanisms and a local equilibrium modeling approach. Water Resour. Res. 1998; 34(12):3293–3302.
12. Brusseau ML, Nelson NT, Oostrom M, Zhang ZH, Johnson GR, Wietsma TW. Influence of heterogeneity and sampling method on aqueous concentrations associated with NAPL dissolution. Environ. Sci. Technol. 2000; 34:3657–3664.
13. Brusseau ML, Zhang Z, Nelson NT, Cain RB, Tick GR, Johnson GR, Oostrom M. Dissolution of nonuniformly distributed immiscible liquid: intermediate-scale experiments and mathematical modeling. Environ. Sci. Technol. 2002; 36:1033–1041. [PubMed: 11917988]
14. Johnson GR, Zhang Z, Brusseau ML. Characterizing and quantifying the impact of immiscible-liquid dissolution and nonlinear, rate-limited sorption/desorption on low-concentration elution tailing. Water Resour. Res. 2003; 39(5):6-1–6-7.
15. Fure AD, Jawitz JW, Annable MD. DNAPL source-zone depletion: linking architecture and response. J. Contam. Hydrol. 2006; 85:118–140. [PubMed: 16527371]
16. Brusseau ML, DiFilippo EL, Marble JC, Oostrom M. Mass-removal and mass-flux-reduction behavior for idealized source zones with hydraulically poorly-accessible immiscible liquid. Chemosphere.
17. Russo AE. Immiscible liquid transport in natural porous media. Dissertation. 2008
18. Brusseau ML. Rate-limited mass-transfer and transport of organic solutes in porous-media that contain immobile immiscible organic liquid. Water Resour. Res. 1992; 28(1):33–45.
19. Soerens TS, Sabatini DA, Harwell JH. Effects of flow bypassing and nonuniform NAPL distribution on the mass transfer characteristics of NAPL dissolution. Water Resour. Res. 1998; 34(7):1657–1673.
20. Hamed MM, Nelson PD. A distributed-site model for non-equilibrium dissolution of multi-component residually trapped NAPL. Environ. Model. Softw. 2000; 15:443–450.
21. Zhang Z, Brusseau ML. Nonideal transport of reactive contaminants in heterogeneous porous media: 7. distributed-domain model incorporating immiscible-liquid dissolution and rate-limited sorption/desorption. J. Contam. Hydrol. 2004; 74:83–103. [PubMed: 15358488]
22. Johns ML, Gladden LF. Magnetic resonance imaging study of the dissolution kinetics of octanol in porous media. J. Colloid Interface Sci. 1999; 210:261–270. [PubMed: 9929413]
23. Johns ML, Gladden LF. Probing ganglia dissolution and mobilization in a water-saturated porous medium using MRI. J. Colloid Interface Sci. 2000; 225:119–127. [PubMed: 10767152]
24. Fontenot MM, Vigil RD. Pore-scale study of nonaqueous phase liquid dissolution in porous media using laser-induced fluorescence. J. Colloid Interface Sci. 2002; 247:481–489. [PubMed: 16290489]
25. Zhang C, Werth CJ, Webb AG. A magnetic resonance imaging study of dense nonaqueous phase liquid dissolution from angular porous media. Environ. Sci. Technol. 2002; 36:3310–3317. [PubMed: 12188359]
26. Schnaar G, Brusseau ML. Characterizing pore-scale dissolution of organic immiscible liquid in natural porous media using synchrotron X-ray microtomography. Environ. Sci. Technol. 2006; 40:6622–6629. [PubMed: 17144287]
27. Schnaar G, Brusseau ML. Pore-scale characterization of organic immiscible-liquid morphology in natural porous media using synchrotron X-ray microtomography. Environ. Sci. Technol. 2005; 39:8403–8410. [PubMed: 16294880]
28. Rivers, ML. GSECARS Tomography software. Web page: http://cars9.uchicago.edu/software/index.html
29. Ketcham RA. Computational methods for quantitative analysis of three-dimensional features in geological specimens. Geosphere. 2005; 1:32–41.
30. Brusseau ML, Peng S, Schnaar G, Constanza-Robinson MS. Relationships among air- water interfacial area, capillary pressure, and water saturation for a sandy porous medium. Water Resour. Res. 2006; 42(3):W03501.

31. Brusseau ML, Peng S, Schnaar G, Murao A. Measuring air-water interfacial areas with x-ray microtomography and interfacial partitioning tracer tests. Env. Sci. Technol. 2007; 41(6):1956–1961. [PubMed: 17410790]

32. Brusseau ML, Janousek H, Murao A, Schnaar G. Synchrotron x-ray microtomography and interfacial partitioning tracer test measurements of NAPL-water interfacial areas. Water Resour. Res. 2008; 44(1):W01411.

33. Al-Roush RI, Wilson CS. A pore-scale investigation of a multiphase porous media system. J. Contam. Hydrol. 2005; 77:67–89. [PubMed: 15722173]

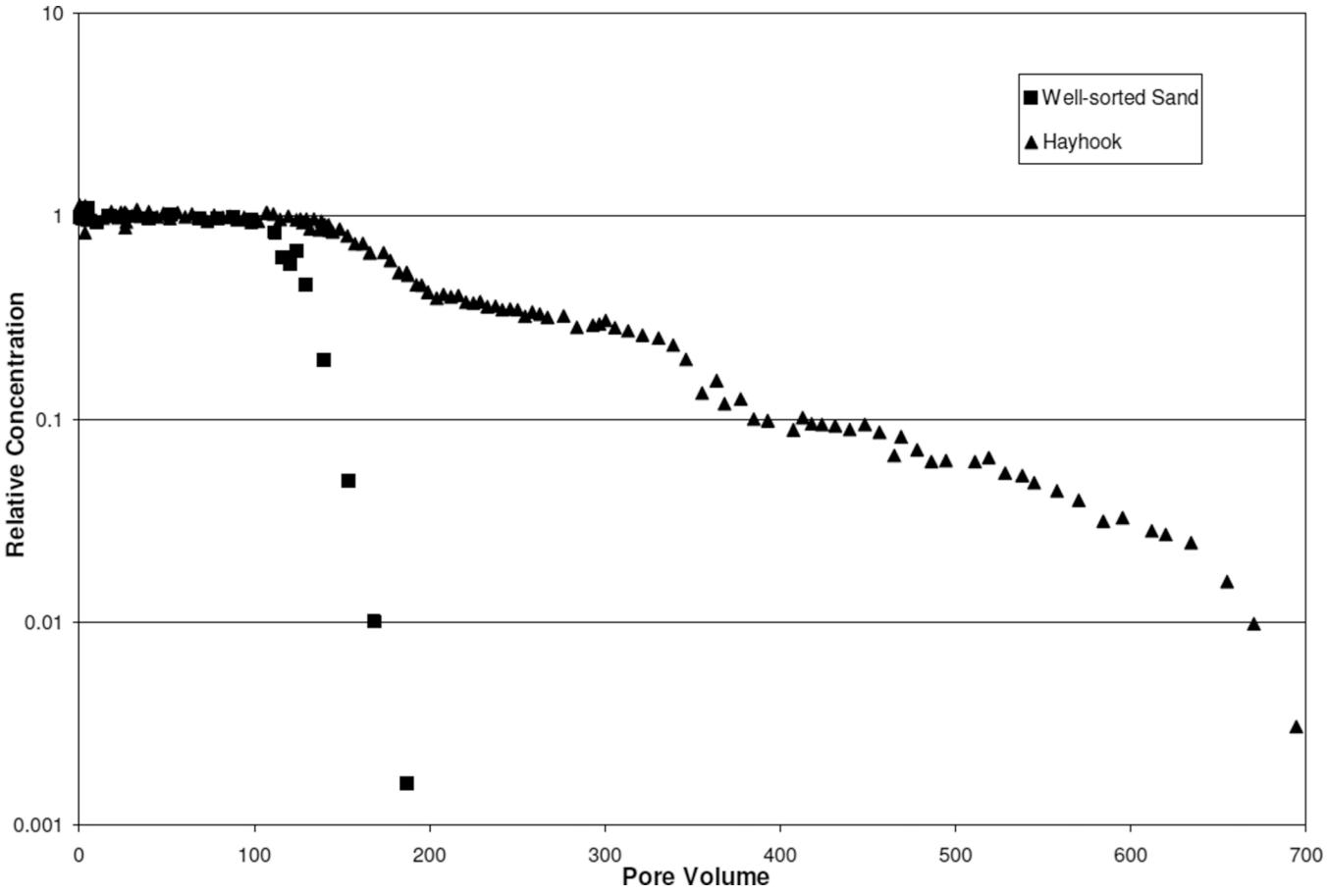

Figure 1.
Elution curves representing essentially complete mass removal for dissolution experiments conducted with a well-sorted sand and a poorly-sorted porous medium (Hayhook soil); data from (17).

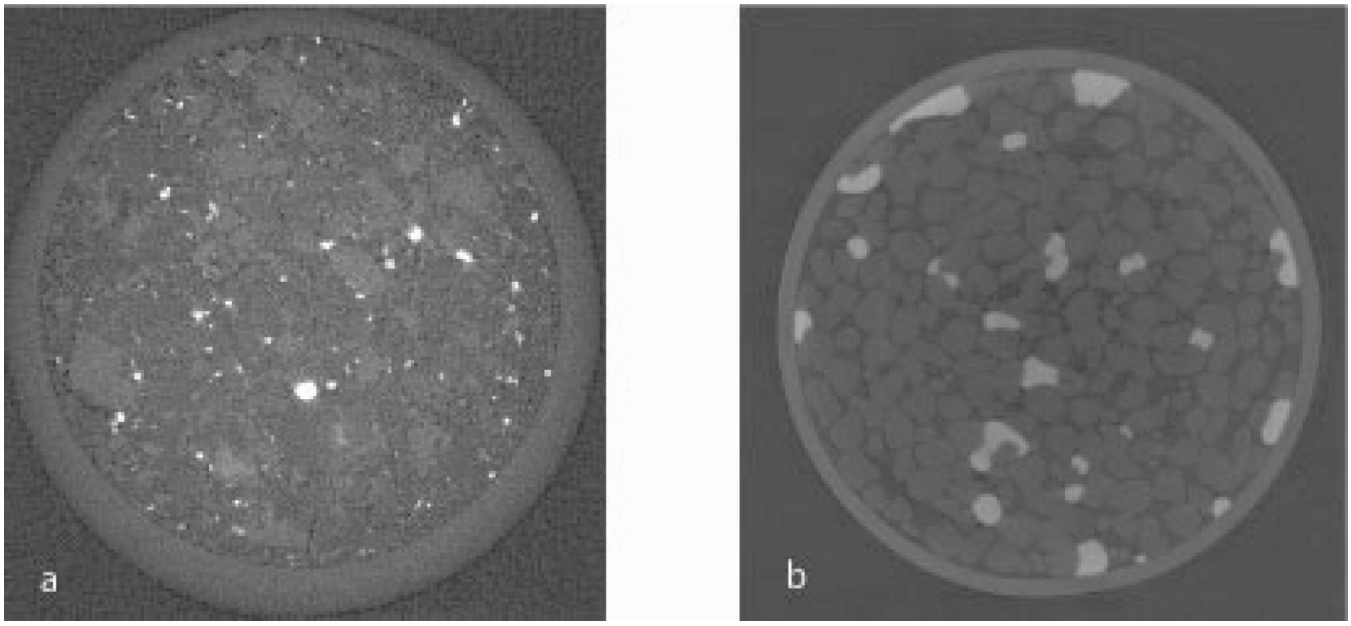

Figure 2.
X-ray microtomography results for Hayhook soil (a) and well-sorted sand (b). Thin sections in the x–y direction (planar view), where organic liquid is white, porous media grains are light gray, and the aqueous phase is dark grey. The column outer diameter is 6.35 mm.

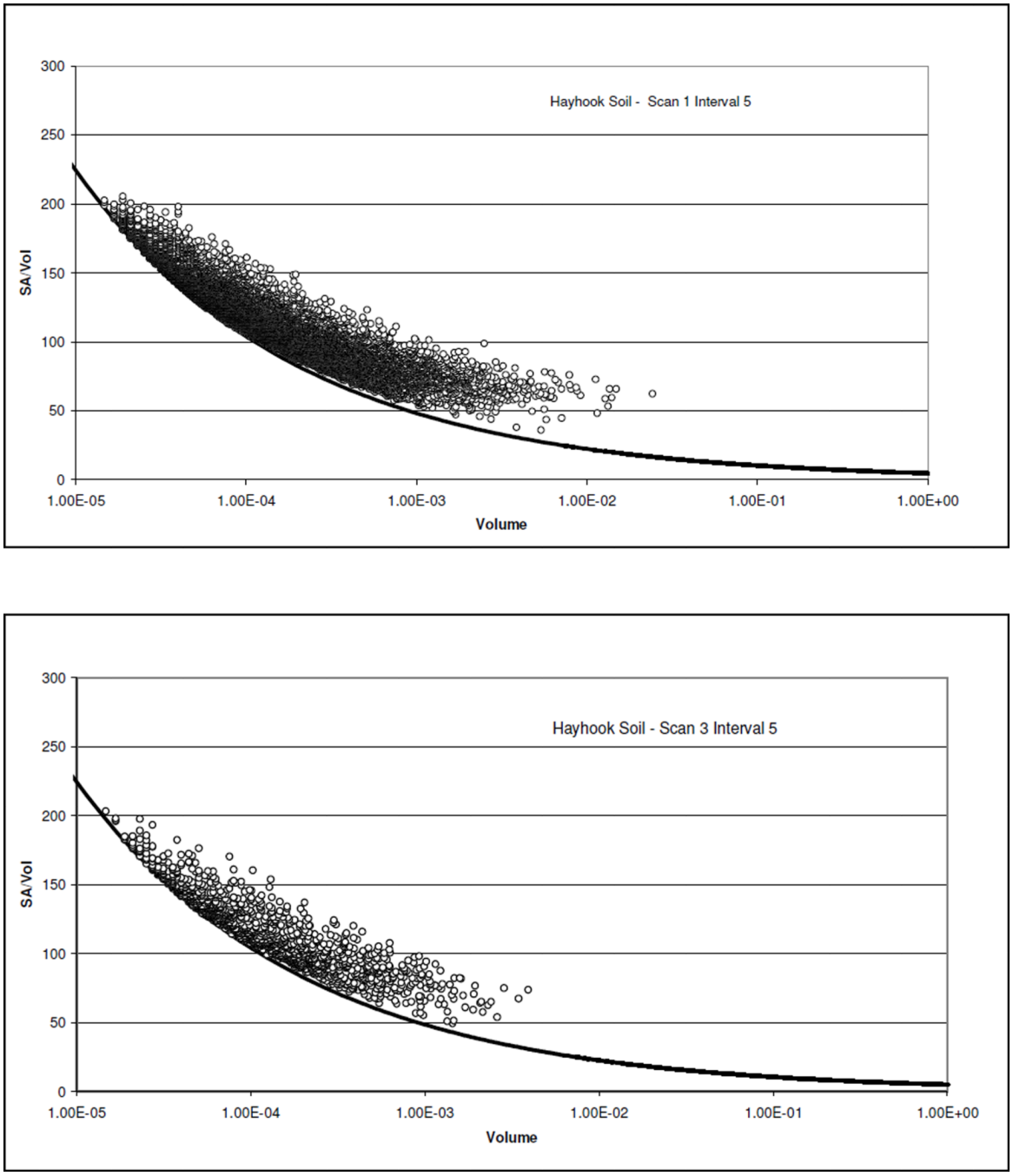

Figure 3.
Organic-liquid blob size distributions for initial scan (top) and third scan (bottom) for dissolution experiment conducted with Hayhook soil. The solid line represents the surface area to volume ratio (SA/VOL) for a perfect sphere.

4A

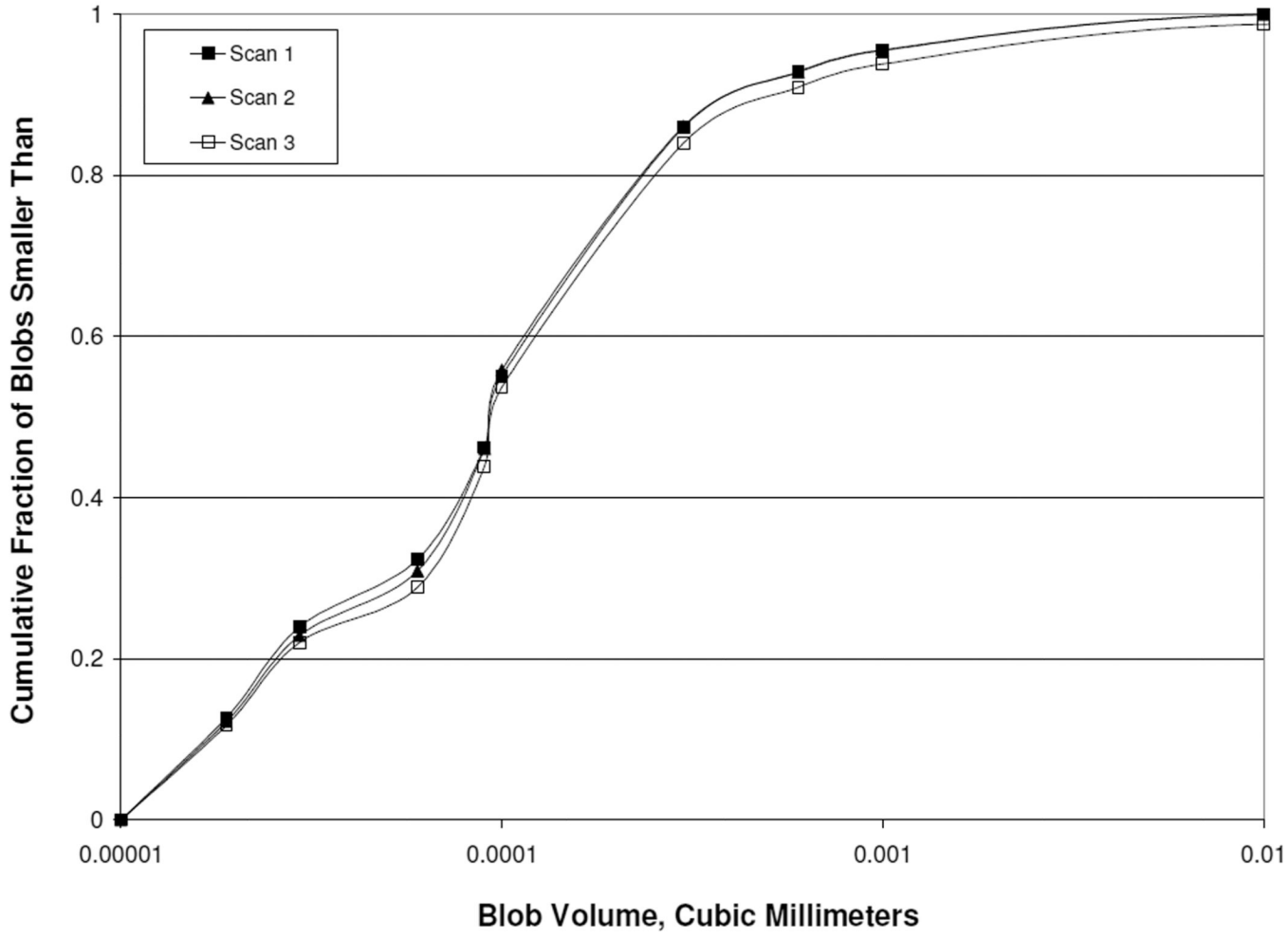

4B

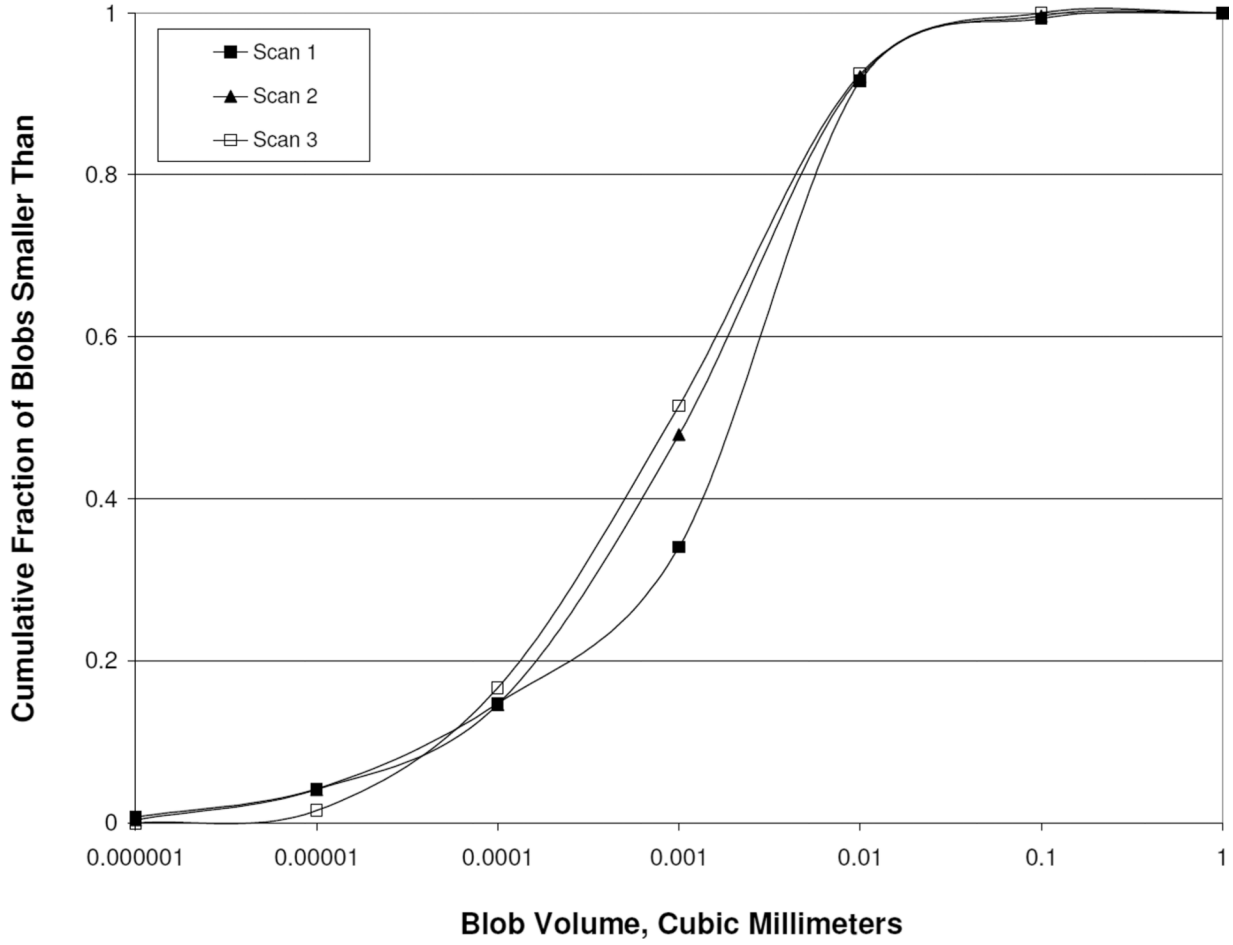

Figure 4.
Cumulative blob-size distributions for the two porous media. A. Hayhook, B. Well-sorted sand.

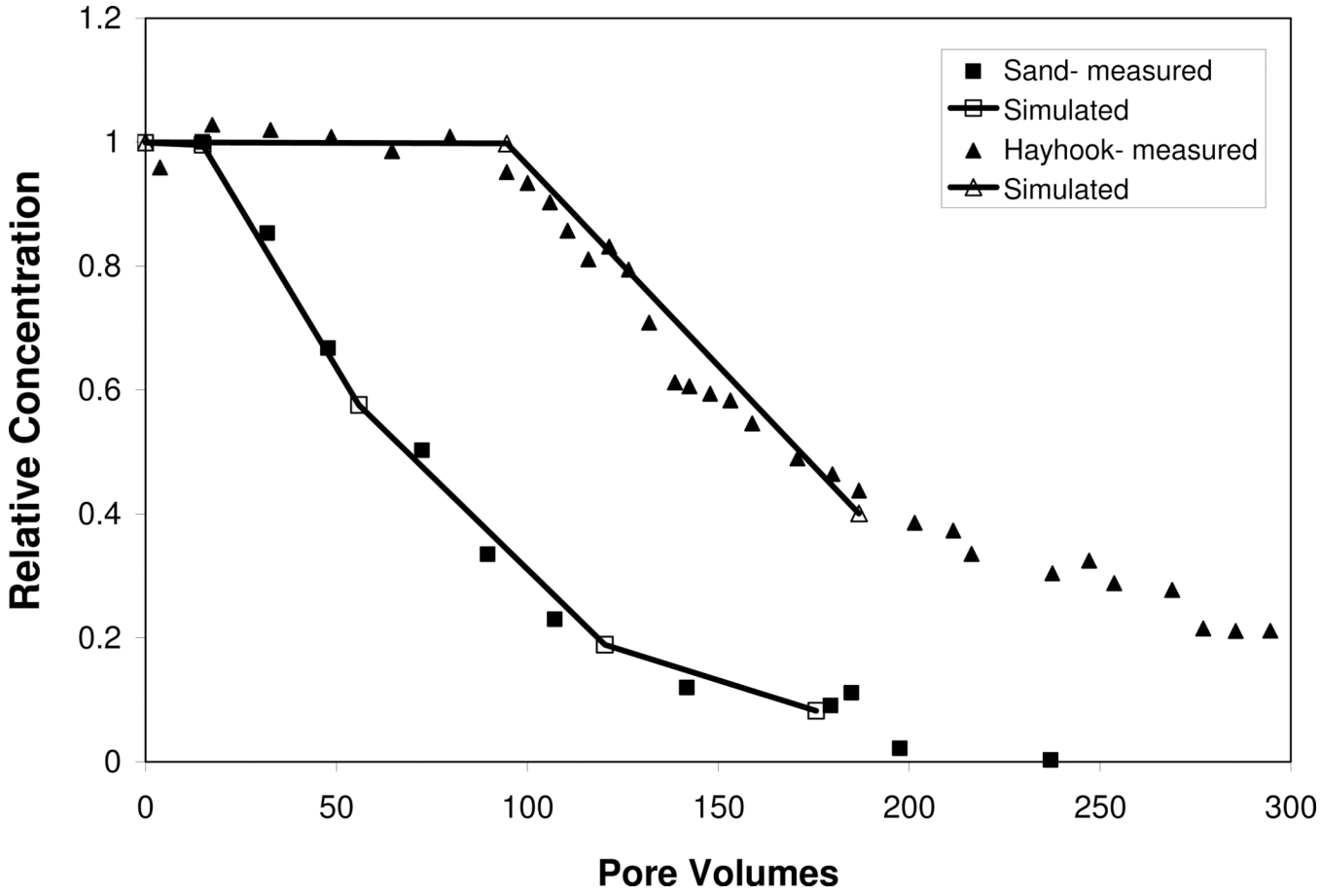

Figure 5.
Measured and simulated elution data for the dissolution experiments. The simulated data were generated with equation 1, wherein interfacial areas were obtained from microtomography and the mass-transfer coefficient was calibrated. The simulated data are truncated at the point for which the last measured interfacial area is available. The open symbols for the simulated curves represent the points for which measured interfacial areas are available. The lines in between the points are included for visualization purposes.

TABLE 1

Microtomography Data[^]

Scans	SA/Vol[*] (cm^{-1})	A_{nw}[†] (cm^{-1})	Median Blob Diameter (mm)	Percent Mass Remaining
Hayhook				
1	846	17.0	0.062	100
2	838	12.9	0.062	60
3	826	9.0	0.063	48
Sand				
1	197	9.5	0.284	100
2	205	4.5	0.248	52
3	201	1.1	0.245	13

[^] Global values for entire column

[*] Surface Area to Volume Ratio for organic-liquid blobs

[†] Specific Organic-liquid/water interfacial area

TABLE 2

Microtomogrpahy Data For Imaged Intervals in Successive Scans (interval 7 is adjacent to the influent end of the column)

	Hayhook Soil				Well-Sorted Sand			
Scan 1								
Interval	**NAPL Volume mm^3**	**Sn**	**Anw cm^{-1}**	**NAPL SA/Vol cm^{-1}**	**NAPL Volume mm^3**	**Sn**	**Anw cm^{-1}**	**NAPL SA/Vol cm^{-1}**
1	4.3	0.08	17.1	821.5	2.3	0.11	6.3	158.3
2	6.5	0.11	21.4	789.6	2.9	0.14	8.4	167.7
3	6.6	0.11	23.6	862.4	2.0	0.10	8.0	228.5
4	5.3	0.09	19.4	874	5.0	0.24	19.4	223.6
5	4.2	0.07	15.4	877.2	2.9	0.14	11.6	236.8
6	2.9	0.05	10.9	901.9	1.7	0.08	6.1	213.3
7	0.8	0.03	5.2	757.4	-	-	-	-
Total/Ave	**30.6**				**16.8**			
Scan 2								
Interval	**Volume mm^3**	**Sn**	**Anw cm^{-1}**	**NAPL SA/Vol**	**Volume mm^3**	**Sn**	**Anw cm^{-1}**	**NAPL SA/Vol**
1	2.4	0.07	13.4	804.5	1.6	0.08	4.3	156.7
2	6.4	0.11	20.9	799.4	2.0	0.10	5.7	164.7
3	4.5	0.07	16.1	873.7	1.0	0.05	4.2	241.4
4	4.7	0.08	16.5	850	2.5	0.12	10.1	239.2
5	2.1	0.04	7.9	901.9	1.2	0.06	5.8	268.9
6	0.8	0.01	2.7	807.2	0.7	0.03	3.0	248.7
7	0	0	0	0	-	-	-	-
Total/Ave	**20.9**				**9.0**			
Scan 3								
Interval	**Volume mm^3**	**Sn**	**Anw cm^{-1}**	**NAPL SA/Vol**	**Volume mm^3**	**Sn**	**Anw cm^{-1}**	**NAPL SA/Vol**
1	2.2	0.06	12.2	803.2	0.5	0.03	1.7	187.0
2	4.9	0.08	16.3	792.5	0.9	0.04	2.5	159.0
3	3.8	0.06	13.7	862.5	0.1	0.01	0.6	280.8
4	3.4	0.06	11.9	841.5	0.4	0.02	1.7	262.4

Environ Sci Technol. Author manuscript; available in PMC 2011 September 2.

	Hayhook Soil				Well-Sorted Sand			
Scan 1								
Interval	**NAPL Volume mm^3**	**Sn**	**Anw cm^{-1}**	**NAPL SA/Vol cm^{-1}**	**NAPL Volume mm^3**	**Sn**	**Anw cm^{-1}**	**NAPL SA/Vol cm^{-1}**
5	0.3	0.01	1.2	919.8	0.3	0.01	1.2	254.1
6	0	0	0	0	0.1	0.01	0.5	235.4
7	0	0	0	0	-	-	-	-
Total/Ave	**14.6**				**2.3**			

NAPL = organic immiscible liquid

S_n = organic liquid saturation

A_{nw} = specific organic-liquid/water interfacial area

SA = surface area of organic liquid

Vol = volume of organic liquid